Published in final edited form as:
Stroke. 2011 July ; 42(7): 2054–2060. doi:10.1161/STROKEAHA.110.597997.

Validation of In Vivo MRI Blood-Brain Barrier Permeability Measurements by Comparison with Gold Standard Histology

Angelika Hoffmann, BS[1,2], **Jörg Bredno, PhD**[3], **Michael F. Wendland, PhD**[2], **Nikita Derugin, MA**[4], **Jason Hom, MD**[2], **Tibor Schuster, PhD**[5], **Hua Su, MD**[6], **Peter T. Ohara, PhD**[7], **William L. Young, MD**[6], and **Max Wintermark, MD**[1,2]

[1]University of Virginia, Department of Radiology, Neuroradiology Division, Charlottesville, VA

[2]University of California San Francisco, Department of Radiology, Neuroradiology Section, San Francisco, CA

[3]Philips Healthcare, CT and Nuclear Medicine, Imaging Physics and System Analysis, San Jose, CA

[4]University of California San Francisco, Department of Neurosurgery, San Francisco, CA

[5]Technische Universität München, Institute of Medical Statistics and Epidemiology, Munich, Germany

[6]University of California San Francisco, Department of Anesthesia and Perioperative Care, San Francisco, CA

[7]University of California San Francisco, Department of Anatomy, San Francisco, CA

Abstract

Background and Purpose—To validate the blood-brain barrier permeability measurements extracted from perfusion-weighted MRI through a relatively simple and frequently applied model, the Patlak model, by comparison with gold standard histology in a rat model of ischemic stroke.

Methods—Eleven spontaneously hypertensive rats and eleven Wistar rats with unilateral, 2h filament occlusion of the right MCA underwent imaging during occlusion, at 4h and 24h post reperfusion. BBB permeability was imaged by gradient echo imaging after the first pass of the contrast agent bolus and quantified by a Patlak analysis. BBB permeability was shown on histology by the extravasation of Evans blue on fluorescence microscopy sections matching location and orientation of MR images. Cresyl-violet staining was used to detect and characterize hemorrhage. Landmark-based elastic image registration allowed a region-by-region comparison of permeability imaging at 24 hours with Evans blue extravasation and hemorrhage as detected on histological slides obtained immediately after the 24-hour image set.

Results—Permeability values in the non-ischemic tissue (marginal mean±SE: 0.15±0.019ml/min·100ml) were significantly lower compared to all permeability values in regions of Evans blue extravasation or hemorrhage. Permeability values in regions of weak Evans blue extravasation (0.23±0.016ml/min·100ml) were significantly lower compared to permeability values of in regions of strong Evans blue extravasation (0.29±0.020ml/min·100ml) and macroscopic hemorrhage (0.35±0.049ml/min·100ml). Permeability values in regions of microscopic hemorrhage

Address for correspondence and reprint requests: Max Wintermark, M.D., Associate Professor of Radiology, Neurology, Neurosurgery and Biomedical Engineering, Chief of Neuroradiology, UVA Department of Radiology, Box 800170, Charlottesville, VA 22908, Phone: 434-243-9312, Fax: 434-982-5753, Max.Wintermark@virginia.edu.

Disclosure: This study was supported by a seed grant from the UCSF Department of Radiology and Biomedical Imaging. Jörg Bredno is an employee of Philips Healthcare.

(0.26±0.024ml/min·100ml) only differed significantly from values in regions of non-ischemic tissue (0.15±0.019 ml/min·100ml).

Conclusion—Areas of increased permeability measured in-vivo by imaging coincide with BBB disruption and hemorrhage observed on gold standard histology.

Keywords

ischemic stroke; hemorrhagic transformation; blood-brain barrier permeability; MRI; validation study

Introduction

Hemorrhagic transformation (HT) is a serious complication of ischemic stroke, which can increase the risk of mortality up to 11 times.[1] Combined data from 6 major stroke trials showed that severe hemorrhage with significant mass effect occurs in 5% of patients with stroke treated with tPA within 3 hours after symptom onset and in up to 6% in patients treated between 3 and 6 hours.[2] HT is a multifactorial phenomenon [3], with damage to the blood-brain barrier (BBB) and subsequent vascular leakage being considered one of the contributing mechanisms.[4, 5] HT can occur spontaneously, but is more often triggered by reperfusion.[3] Oxidative stress occurs very early after ischemia and is accrued by reperfusion. It causes damage to lipid-rich membranes in the BBB, and consequently leads to vascular leakage and possibly vascular disruption in ischemic brain tissue. [6, 7] Additionally, oxidative stress stimulates inflammatory cytokine production and protease secretion by microglia, infiltrating leucocytes and resident cells of the neurovascular unit.[8, 9] As these neuroinflammatory mechanisms become activated, alterations in cytokine profiles, adhesion-molecule expression and tight junction components mediate further vascular leakage.[3] Although many proteases are expressed in the brain under normal and ischemic conditions, both animal and human studies suggest that the matrix metalloproteinase family and the tPA system play a central role in activating the proteolysis cascade.[10–13]

Early detection of a damaged BBB by imaging could potentially be used to identify patients who are more likely to develop HT, and would impact the selection of patients with ischemic stroke for acute reperfusion therapies.[14–18] Measurement of BBB permeability using perfusion imaging relies on applying a mathematical model to the time-signal curves of an intravascular, partly permeating tracer recorded on the images. A mathematical model is always a simplified representation of the reality summarized by an equation. As long as assumptions underlying the model are respected, results are supposed to be correct, but cannot necessarily be considered as definite, and validation against a gold standard is required.

The goal of this study is to validate BBB permeability measurements extracted from perfusion-weighted MRI through a relatively simple and frequently applied model, the Patlak model [19, 20], by comparison with gold standard histology in a rat model of ischemic stroke.

Material and Methods

Study design

The experimental animals were cared for in accordance with the Animal Welfare Act, and the experiments conducted in compliance with our institutional guidelines for animal research and with the approval of the University of California San Francisco Committee on Animal Research.

Spontaneously hypertensive (SHR) male rats and Wistar male rats of 220–280 grams (Charles River laboratory) were subjected to a 2h filament occlusion of the right middle cerebral artery. MR imaging was obtained during occlusion, as well as 4h and 24h after reperfusion.

All experiments – surgery and MR imaging - were conducted while the animals were anesthetized. Anesthesia was induced by isofluerane 3.5% and then maintained at 2%. Immediately after the 24-hour MRI scan, the animal was injected with Evans blue (Sigma Chemical Co, St. Louis, Missouri, USA; 0.6ml of a 2% solution in saline), which circulated for 30min. After the circulation period the animals were euthanized by decapitation, the brain was quickly removed and then prepared for histological processing.

Animal Surgery

Reversible middle cerebral artery occlusion was performed according to a previously described technique [21]. In brief, we inserted a precoated suture (7.0, Ethicon) through the external carotid artery (ECA) into the internal carotid artery (ICA). The suture was advanced 18–23mm past the ECA-ICA bifurcation to occlude the MCA. MCA occlusion and associated ischemic injury were confirmed during occlusion by perfusion- and diffusion-weighted MRI. Reperfusion of the MCA territory was achieved by withdrawal of the suture 2 hours after occlusion.

MR Imaging

The MRI was performed with a 2T Bruker Omega CSI system (Bruker Instruments Inc., Freemont, CA) equipped with Acustar S-150 self-shielded gradients (+/− 20G/cm, 15cm inner diameter). The animals were placed supine on a plastic support with ear and bite bars to minimize head motion during breathing. The head was inserted into a custom 5.5-cm diameter birdcage transmit–receive imaging coil. A water-recirculating warming pad was wrapped around the animal below the neck to maintain body temperature at 37°C, as monitored by an intrarectal thermocouple.

The MRI protocol was the same at each timepoint (during occlusion, as well as 4h and 24h after reperfusion) and included the sequences listed in Supplemental Table 1 (online only). All images were obtained in the coronal plane, were obtained as 8 consecutive 2mm slices (if not otherwise specified), and an image matrix size of 128×128 pixels.

In order to achieve quantitative hemodynamic measurements of cerebral perfusion and permeability, two boluses were injected. The first bolus of contrast was administered to measure permeability and served as a pre-load bolus for the perfusion scans, performed with a second bolus of contrast. As shown previously [22], this preloading minimizes the effect of contrast leakage for the perfusion imaging.

Image Processing

The brain parenchymal tissue was segmented by intensity thresholding on the T2-weighted images. All subsequent processing was limited to the voxels belonging to the brain parenchymal tissue mask determined by segmentation.

Perfusion maps were computed using a commercially available software (Brain Perfusion, Extended Brilliance Workspace, Philips Healthcare, Cleveland, OH, USA) that was modified in a tailored fashion for the purpose of this research project. This software relies on the central volume principle, which is the most accurate for low injection rates of iodinated contrast material [23]. After motion correction and noise reduction by an anisotropic, edge-preserving spatial filter, the software applies curve fitting by least mean squares to obtain

mathematical descriptions of the time-density curves for each pixel. The cerebral blood volume (CBV) map is calculated from the area under the time-density curves compared to a similarly obtained venous reference curve [24]. A closed-form deconvolution is then applied to calculate the mean transit time (MTT) map [25]. The deconvolution operation requires a reference arterial input function that was manually selected. This closed-form deconvolution provides MTT maps even for animal data with a mean transit time in brain tissue of 1.5s close to the sampling rate of 1s, which is a known challenge for all perfusion algorithms. The cerebral blood flow (CBF) was computed as: CBF = CBV/MTT.

For the computation of permeability maps, the superior sagittal sinus was manually selected to provide the reference time-concentration curve for the intravascular contrast agent concentration. Permeability maps were computed by Patlak analysis[19,20], which provides the estimation of a local CBV together with the blood-to-brain transfer constant k_1. The analysis included an additional stabilizing step where the area under the reference curve was scaled such that a target median CBV of 3ml/100g was obtained in the contralateral hemisphere for all animals at all timepoints.

Histopathology

Frozen tissue sections of 50μm were cut on a cryostat (Leica Microsystems, Wetzlar, Germany), from Bregma −5mm to +2mm [26], covering all regions possibly affected by infarction. Every 500μm, two sections were collected and used for Cresyl-violet staining and fluorescent microscopy analyses.

Image Analysis: Infarction and Hemorrhage

Sections stained with Cresyl-violet were examined microscopically with varying magnifications to delineate infarction and to identify different types of hemorrhagic transformation.

The infarction was identified on the Cresyl-violet section on light microscopy as a region of pallor that contained shrunken cell bodies characteristic of neuronal cell death.

Macroscopic hemorrhage was defined as blood visible without magnification and confirmed by higher magnification (20×). Microscopic hemorrhage was defined as blood only visible by microscopy (20×) [27] showing tissue characteristics of a petechial bleed (Supplemental Figure 1). Such regions usually showed co-location of extravascular red blood cells in the structurally preserved brain tissue with or without plugging of cerebral microvessels with red blood cells, as well as formation of small blood clots by the extravasated blood.

Image Analysis: Extravasation of Evans Blue

Fluoroscopy images were used to identify the Evans blue marker on all sections. Images were examined on a standard fluorescent microscope using a Nikon CY3 filter set. Images were digitally captured with a digital microscope camera AxioCam IC (Carl Zeiss AG, Germany). Strong and weak appearance of Evans blue were distinguished by identifying regions where more than 50% or less than 50% of visible cells had taken up the marker.

Alignment of In-Vivo Imaging and Histology

For all histology sections, overview images showing the whole brain were created using an in-house Matlab application (The MathWorks, Inc., Natick, MA) that allows stitching of multiple low-power images. All ROIs identified directly at the microscope (infarction, macroscopic and microscopic hemorrhage, strong and weak extravasation of Evans blue) were transferred onto the overview images using Matlab.

The in-vivo and histology images were obtained almost simultaneously, approximately 30 minutes apart. However, in order to address a possible evolution in the degree of hemispheric brain swelling, and deformation of the specimen occurring during the histology processing, in-vivo and histology image data were coregistered based on an anatomical atlas of the rat brain [26]. Eighteen distinct slices from this atlas were selected that axially covered all imaged brain regions. A set of 20 landmarks was selected that was visible on histology sections and the T2-weighted MRI images. A multi-step elastic registration process was designed and implemented so that individual brain hemispheres and manually defined ROIs on all slices were aligned to their corresponding atlas slices. ROIs defined on ground truth microscopy slides were made available on the in-vivo permeability and perfusion maps (Figure 1).

Once registration was completed, permeability values in the ROIs delineating the infarction and hemorrhages (macroscopic and microscopic) were recorded. CBF, CBV and MTT values within these ROIs were also recorded. CBF, CBV, MTT and permeability values were also recorded in the contralateral, nonischemic hemisphere.

To assess the accuracy of the registration process, one experienced observer (AH) marked the position of visible anatomical structures separately and in a blinded fashion on selected Cresyl-violet sections and on the atlas. The average distance between the location of these structures on the Cresyl-violet sections and their location on the atlas, considered as the reference, was calculated.

Statistical analysis

Permeability values in the macroscopic and microscopic hemorrhagic ROIs, in the strong and weak Evans blue ROIs were compared using a linear mixed regression model to values in the contralateral, nonischemic hemisphere or values in the infarcted hemisphere, but outside the drawn ROIs. The linear mixed regression model approach proper reflects the structure of repeated data and takes correlations of multiple measurements per individual rat into account. Marginal means for the different ROIs were reported with standard errors (±SE).

Non-parametric Mann-Whitney U tests were used to compare quantitative data between SHR and Wistar rat groups. Quantitative data was described using average, standard deviation (SD) and range. All statistical tests were performed two-sided and a p-value less than 0.05 was considered statistically significant.

Results

Study population

Eleven male SHR rats and eleven male Wistar rats of 220–280 grams (Charles River laboratory) were subjected to a 2h filament occlusion of the right middle cerebral artery. MR imaging was obtained during occlusion, as well as 4h and 24h after reperfusion. The present study focuses on the MR imaging obtained 24h after reperfusion, just before injection of Evans blue and euthanization. The MR imaging during occlusion was used to confirm the inclusion of the animals in the study. The MR imaging obtained at 4 hours after reperfusion was used to assess the degree of reperfusion.

Animals were excluded from the study if the perfusion imaging showed no reperfusion or if the DWI lesion during occlusion involved only subcortical regions, but not the cortex. Seven normal Wistar and 1 spontaneously hypertensive rats were excluded because of this criteria. One additional SHR rat was excluded, as it died shortly after reperfusion due to vessel

perforation. The characteristics of the remaining 9 male SHR rats and 4 male Wistar rats are described in Table 1.

Infarct characteristics

The same final infarction pattern was obtained in the Wistar and SHR rats, both on DWI images at 24h and on the Cresyl-violet sections. The infarction patterns for Wistar and SHR rats are presented in Supplemental Figure 2 and show similar distribution of the infarcted area in both groups of rats.

Reperfusion

Four hours after removal of the suture, reperfusion was examined on perfusion-weighted imaging at 4 hours after removal of the suture (Supplemental Figure 3). All animals but two showed reperfusion from 72% up to 99% (Table 1). One SHR rat did not reperfuse at all as the coating of the occluding filament remained at the origin of the MCA.

Macroscopic and microscopic hemorrhage on histology

Macroscopic hemorrhage occurred more frequently in SHR rats compared to Wistar rats. Macroscopic hemorrhage covered 1% of the hemisphere in SHR rats and 0.1% of the hemisphere in Wistar rats (statistically significant difference: p=0.02) (Table 1)

Microscopic hemorrhage tended to be present at 24 hours post reperfusion with a higher frequency in the SHR rat group, but the difference was not statistically significant (5% in SHR rats versus 2% in Wistar rats, p = 0.22) (Table 1).

Evans blue extravasation on histology

Strong rates of Evans blue extravasation covered 5% of the hemisphere in Wistar rats and 2% in SHR rats (p = 0.41). Weak Evans blue extravasation covered 7% of the hemisphere in Wistar rats and 3% in SHR rats (p = 0.23) (Table 1).

Alignment of In-Vivo Imaging and Histology

From a total of 297 observations on 33 systematically selected Cresyl-violet slices, we determined the overall accuracy of registration as 0.34±0.28mm. This corresponds to approximately 1.1 voxels on the permeability maps. Accuracy of registration was 0.13±0.14mm (≈ 0.4 voxels), 0.38±0.22mm (≈ 1.3 voxels), and 0.30±0.27mm (≈ 1 voxel) in the cortex, preoptic area and striatum, respectively.

Permeability values in different types of ROIs

Both Wistar and SHR rats, showed an average of 5% of increased permeability values at the 24 hour post reperfusion scan. There was no statistical difference of the two groups (p = 0.70) (Table 1).

Permeability values were measured in the six different types of ROIs: non-ischemic, infarct side but outside the drawn ROIs, strong extravasation of Evans blue, weak extravasation of Evans blue, microscopic hemorrhage, and macroscopic hemorrhage.

Permeability values in the non-ischemic tissue (0.15±0.019ml/min·100ml) and permeability values on the infarct side outside the regions of interest (0.18±0.018 ml/min·100ml) were significantly lower compared to permeability values in regions of Evans blue extravasation or hemorrhage. Permeability values in regions of weak Evans blue extravasation (0.23±0.016ml/min·100ml) were significantly lower compared to permeability values of in regions of strong Evans blue extravasation (0.29±0.020ml/min·100ml) and macroscopic

hemorrhage (0.35±0.049ml/min·100ml). Permeability values in regions of microscopic hemorrhage (0.26±0.024ml/min·100ml) only differed significantly from values in regions of non-ischemic tissue Permeability values in the non-ischemic tissue (marginal mean±SE: 0.15±0.019ml/min·100ml) and permeability values on the infarct side outside the regions of interest (0.18±0.18 ml/min·100ml) were significantly lower compared to all permeability values in regions of Evans blue extravasation or hemorrhage. Permeability values in regions of weak Evans blue extravasation (0.23±0.016ml/min·100ml) were significantly lower compared to permeability values of in regions of strong Evans blue extravasation (0.29±0.020ml/min·100ml) and macroscopic hemorrhage (0.35±0.049ml/min·100ml). Permeability values in regions of microscopic hemorrhage (0.26±0.024ml/min·100ml) only differed significantly from values on the infarct side outside the regions of interest (0.18±0.18 ml/min·100ml) or values in regions of non-ischemic tissue (0.15±0.019 ml/min·100ml).(Figure 2, Table 2).

The permeability values in the different regions of interest were not significantly different in SHR and Wistar rats.

Discussion

The purpose of this study was to validate in-vivo BBB permeability measurements extracted from perfusion-weighted MRI by the same software that has been used in acute stroke patients [28–31] by comparison with gold standard histology. This software relies on the Patlak model to calculate BBB permeability values, and has been used to predict clinically significant hemorrhagic transformation in acute stroke patients receiving tPA[32].

Our results indicate that all areas of BBB disruption (Evans blue extravasation and hemorrhages) identified on histology have significantly increased permeability on imaging compared to non-affected brain. Permeability imaging is also able to grade the degree of BBB disruption, as regions with strong Evans blue extravasation shows higher permeability on imaging compared to regions with weak Evans blue extravasation. Permeability values on imaging were very similar in regions with strong Evans blue extravasation and in regions with macroscopic hemorrhage.

For the present study, we focused on the 24h timepoint in order to validate the BBB permeability measurements. At 24h post reperfusion, histological signs of an ischemic injury have developed, the endothelium is severely damaged and BBB disruption has occurred. The ruptured BBB was detected by injecting Evans blue right after the last imaging scan and which circulated for 30 minutes. This study being a cross-sectional study comparing imaging and histology obtained almost simultaneously at 24 hours does not allow inferences to be made about the causal relationship between increased BBB permeability and hemorrhagic transformation in the setting of acute ischemic stroke.

In order to achieve our validation goal, we thought it important to work on a dataset that included intact BBB values together with a wide range of permeable and disrupted BBB values. The hemispheric stroke model selected for this study reliably induced ischemic stroke with a diffusion lesion that affected 79 percent of the selected hemisphere in SHR rats and 80 percent in Wistar rats. The two different breeds, Wistar and SHR rats, were selected so that the same 2h MCA occlusion could result in different degrees of BBB disruption and of hemorrhagic transformation, despite similar infarct size at 24 hours post-reperfusion to brain tissue. SHR rats were more likely to develop macroscopic hemorrhage compared to Wistar rats, which is in agreement with previously performed studies [27, 33, 34]. However, the permeability values were not significantly different in SHR and Wistar rats, which might be due to the small sample size. Further investigation will be necessary to address this issue.

While this study shows the sensitivity of in-vivo BBB measurements by imaging, it also identifies limitations. Imaging assessment of the BBB permeability cannot distinguish between different reasons for contrast agent extravasation, namely permeation through an open BBB in otherwise intact vasculature and leakage of contrast agent through damaged vascular walls.

An additional limitation of this study is that Gd-DTPA (molecular weight 552 Da) and Evans blue tagged albumin (~68kDa) differ in size and distribution volumes. Different extravasation mechanisms for both agents are also described in vitro and in vivo studies under condition of hypoxia.[35, 36] However, a reperfusion injury after 2h middle cerebral artery occlusion produces extensive damage to the whole neurovascular unit including tight junctions and endothelial cells. Therefore, even if the amount of extravasated Gd-DTPA and Evans blue tagged albumin may be different due to their respective sizes, we observed that the locations of Evans blue leakage on histology and areas with increased permeability values on Gd-DTPA imaging, were the same, and as such our comparison of the two is justified. Gd-DTPA can be linked to bovine serum albumine (BSA) and Evans blue and then has similar properties and a similar extravasation mechanism to Evans blue. Gd-BSA-EB has been studied in the setting of BBBP in ischemic stroke,[37] but was not used in this study in order to stick to the same imaging method already used in patients.

Using a contrast agent with similar properties as Evans blue, e.g. Gd-BSA-EB, which has been studied in the settings of ischemic stroke[37],

In conclusion, this study validates that regions of increased permeability measured in-vivo by imaging coincide with BBB disruption and hemorrhage observed on gold standard histology. The imaging method that was used to assess BBB permeability disruption was exactly the same as the one used previously in patients with acute ischemic stroke in order to predict hemorrhagic transformation after administration of tPA.

Supplementary Material

Refer to Web version on PubMed Central for supplementary material.

Acknowledgments

This study was supported by a seed grant from the UCSF Department of Radiology and Biomedical Imaging.

Jörg Bredno is an employee of Philips Healthcare.

References

1. Berger C, Fiorelli M, Steiner T, Schabitz WR, Bozzao L, Bluhmki E, Hacke W, von Kummer R. Hemorrhagic transformation of ischemic brain tissue: Asymptomatic or symptomatic? Stroke. 2001; 32:1330–1335. [PubMed: 11387495]
2. Hacke W, Donnan G, Fieschi C, Kaste M, von Kummer R, Broderick JP, Brott T, Frankel M, Grotta JC, Haley EC Jr, Kwiatkowski T, Levine SR, Lewandowski C, Lu M, Lyden P, Marler JR, Patel S, Tilley BC, Albers G, Bluhmki E, Wilhelm M, Hamilton S. Association of outcome with early stroke treatment: Pooled analysis of atlantis, ecass, and ninds rt-pa stroke trials. Lancet. 2004; 363:768–774. [PubMed: 15016487]
3. Wang X, Lo EH. Triggers and mediators of hemorrhagic transformation in cerebral ischemia. Mol Neurobiol. 2003; 28:229–244. [PubMed: 14709787]
4. Lyden PD, Zivin JA. Hemorrhagic transformation after cerebral ischemia: Mechanisms and incidence. Cerebrovasc Brain Metab Rev. 1993; 5:1–16. [PubMed: 8452759]

5. Lapchak PA. Hemorrhagic transformation following ischemic stroke: Significance, causes, and relationship to therapy and treatment. Curr Neurol Neurosci Rep. 2002; 2:38–43. [PubMed: 11898581]
6. Chan PH. Oxygen radicals in focal cerebral ischemia. Brain Pathol. 1994; 4:59–65. [PubMed: 8025703]
7. Gursoy-Ozdemir Y, Can A, Dalkara T. Reperfusion-induced oxidative/nitrative injury to neurovascular unit after focal cerebral ischemia. Stroke. 2004; 35:1449–1453. [PubMed: 15073398]
8. Haddad JJ. Redox regulation of pro-inflammatory cytokines and ikappab-alpha/nf-kappab nuclear translocation and activation. Biochem Biophys Res Commun. 2002; 296:847–856. [PubMed: 12200125]
9. Inoue N, Takeshita S, Gao D, Ishida T, Kawashima S, Akita H, Tawa R, Sakurai H, Yokoyama M. Lysophosphatidylcholine increases the secretion of matrix metalloproteinase 2 through the activation of nadh/nadph oxidase in cultured aortic endothelial cells. Atherosclerosis. 2001; 155:45–52. [PubMed: 11223425]
10. Planas AM, Sole S, Justicia C. Expression and activation of matrix metalloproteinase-2 and -9 in rat brain after transient focal cerebral ischemia. Neurobiol Dis. 2001; 8:834–846. [PubMed: 11592852]
11. Rosell A, Ortega-Aznar A, Alvarez-Sabin J, Fernandez-Cadenas I, Ribo M, Molina CA, Lo EH, Montaner J. Increased brain expression of matrix metalloproteinase-9 after ischemic and hemorrhagic human stroke. Stroke. 2006; 37:1399–1406. [PubMed: 16690896]
12. Rosenberg GA, Navratil M, Barone F, Feuerstein G. Proteolytic cascade enzymes increase in focal cerebral ischemia in rat. J Cereb Blood Flow Metab. 1996; 16:360–366. [PubMed: 8621740]
13. Sole S, Petegnief V, Gorina R, Chamorro A, Planas AM. Activation of matrix metalloproteinase-3 and agrin cleavage in cerebral ischemia/reperfusion. J Neuropathol Exp Neurol. 2004; 63:338–349. [PubMed: 15099024]
14. Bang OY, Buck BH, Saver JL, Alger JR, Yoon SR, Starkman S, Ovbiagele B, Kim D, Ali LK, Sanossian N, Jahan R, Duckwiler GR, Vinuela F, Salamon N, Villablanca JP, Liebeskind DS. Prediction of hemorrhagic transformation after recanalization therapy using t2*-permeability magnetic resonance imaging. Ann Neurol. 2007; 62:170–176. [PubMed: 17683090]
15. Lin K, Kazmi KS, Law M, Babb J, Peccerelli N, Pramanik BK. Measuring elevated microvascular permeability and predicting hemorrhagic transformation in acute ischemic stroke using first-pass dynamic perfusion ct imaging. AJNR Am J Neuroradiol. 2007; 28:1292–1298. [PubMed: 17698530]
16. Latour LL, Kang DW, Ezzeddine MA, Chalela JA, Warach S. Early blood-brain barrier disruption in human focal brain ischemia. Ann Neurol. 2004; 56:468–477. [PubMed: 15389899]
17. Aviv RI, d'Esterre CD, Murphy BD, Hopyan JJ, Buck B, Mallia G, Li V, Zhang L, Symons SP, Lee TY. Hemorrhagic transformation of ischemic stroke: Prediction with ct perfusion. Radiology. 2009; 250:867–877. [PubMed: 19244051]
18. Hjort N, Wu O, Ashkanian M, Solling C, Mouridsen K, Christensen S, Gyldensted C, Andersen G, Ostergaard L. Mri detection of early blood-brain barrier disruption: Parenchymal enhancement predicts focal hemorrhagic transformation after thrombolysis. Stroke. 2008; 39:1025–1028. [PubMed: 18258832]
19. Patlak CS, Blasberg RG, Fenstermacher JD. Graphical evaluation of blood-to-brain transfer constants from multiple-time uptake data. J Cereb Blood Flow Metab. 1983; 3:1–7. [PubMed: 6822610]
20. Patlak CS, Blasberg RG. Graphical evaluation of blood-to-brain transfer constants from multiple-time uptake data. Generalizations. J Cereb Blood Flow Metab. 1985; 5:584–590. [PubMed: 4055928]
21. Longa EZ, Weinstein PR, Carlson S, Cummins R. Reversible middle cerebral artery occlusion without craniectomy in rats. Stroke. 1989; 20:84–91. [PubMed: 2643202]
22. Wintermark M, Sesay M, Barbier E, Borbely K, Dillon WP, Eastwood JD, Glenn TC, Grandin CB, Pedraza S, Soustiel JF, Nariai T, Zaharchuk G, Caille JM, Dousset V, Yonas H. Comparative overview of brain perfusion imaging techniques. Stroke. 2005; 36:e83–99. [PubMed: 16100027]

23. Wintermark M, Maeder P, Thiran JP, Schnyder P, Meuli R. Quantitative assessment of regional cerebral blood flows by perfusion ct studies at low injection rates: A critical review of the underlying theoretical models. Eur Radiol. 2001; 11:1220–1230. [PubMed: 11471616]
24. Ladurner G, Zilkha E, Iliff D, du Boulay GH, Marshall J. Measurement of regional cerebral blood volume by computerized axial tomography. J Neurol Neurosurg Psychiatry. 1976; 39:152–158. [PubMed: 1262889]
25. Axel L. Tissue mean transit time from dynamic computed tomography by a simple deconvolution technique. Invest Radiol. 1983; 18:94–99. [PubMed: 6832937]
26. Paxinos, G.; Watson, C. The rat brain in stereotaxic coordinates - the new coronal set. 5. Burlington, MA; San Diego, CA; London, UK: Elsevier Academic Press; 2005. p. 1-209.
27. Ding G, Nagesh V, Jiang Q, Zhang L, Zhang ZG, Li L, Knight RA, Li Q, Ewing JR, Chopp M. Early prediction of gross hemorrhagic transformation by noncontrast agent mri cluster analysis after embolic stroke in rat. Stroke. 2005; 36:1247–1252. [PubMed: 15879323]
28. Dankbaar JW, Hom J, Schneider T, Cheng SC, Lau BC, van der Schaaf I, Virmani S, Pohlman S, Wintermark M. Age- and anatomy-related values of blood-brain barrier permeability measured by perfusion-ct in non-stroke patients. J Neuroradiol. 2009; 36:219–227. [PubMed: 19251320]
29. Hom J, Dankbaar JW, Schneider T, Cheng SC, Bredno J, Wintermark M. Optimal duration of acquisition for dynamic perfusion ct assessment of blood-brain barrier permeability using the patlak model. AJNR Am J Neuroradiol. 2009; 30:1366–1370. [PubMed: 19369610]
30. Dankbaar JW, Hom J, Schneider T, Cheng SC, Lau BC, van der Schaaf I, Virmani S, Pohlman S, Dillon WP, Wintermark M. Dynamic perfusion ct assessment of the blood-brain barrier permeability: First pass versus delayed acquisition. AJNR Am J Neuroradiol. 2008; 29:1671–1676. [PubMed: 18635616]
31. Dankbaar JW, Hom J, Schneider T, Cheng SC, Lau BC, van der Schaaf I, Virmani S, Pohlman S, Dillon WP, Wintermark M. Accuracy and anatomical coverage of perfusion ct assessment of the blood-brain barrier permeability: One bolus versus two boluses. Cerebrovasc Dis. 2008; 26:600–605. [PubMed: 18946215]
32. Hom, J.; Dankbaar, JW.; Soares, BP.; Schneider, T.; Cheng, SC.; Bredno, J.; Lau, BC.; Smith, W.; Dillon, WP.; Wintermark, M. [Accessed December 28, 2010] Blood-brain barrier permeability assessed by perfusion ct predicts symptomatic hemorrhagic transformation and malignant edema in acute ischemic stroke. AJNR Am J Neuroradiol. 2010. [published online ahead of print November 24, 2010]http://www.ajnr.org/pap.dtl
33. Asahi M, Asahi K, Wang X, Lo EH. Reduction of tissue plasminogen activator-induced hemorrhage and brain injury by free radical spin trapping after embolic focal cerebral ischemia in rats. J Cereb Blood Flow Metab. 2000; 20:452–457. [PubMed: 10724108]
34. Neumann-Haefelin C, Brinker G, Uhlenkuken U, Pillekamp F, Hossmann KA, Hoehn M. Prediction of hemorrhagic transformation after thrombolytic therapy of clot embolism: An mri investigation in rat brain. Stroke. 2002; 33:1392–1398. [PubMed: 11988620]
35. Plateel M, Teissier E, Cecchelli R. Hypoxia dramatically increases the nonspecific transport of blood-borne proteins to the brain. J Neurochem. 1997; 68:874–877. [PubMed: 9003080]
36. Sood R, Yang Y, Taheri S, Candelario-Jalil E, Estrada EY, Walker EJ, Thompson J, Rosenberg GA. Increased apparent diffusion coefficients on mri linked with matrix metalloproteinases and edema in white matter after bilateral carotid artery occlusion in rats. J Cereb Blood Flow Metab. 2009; 29:308–316. [PubMed: 18941468]
37. Nagaraja TN, Karki K, Ewing JR, Croxen RL, Knight RA. Identification of variations in blood-brain barrier opening after cerebral ischemia by dual contrast-enhanced magnetic resonance imaging and t 1sat measurements. Stroke. 2008; 39:427–432. [PubMed: 18174480]

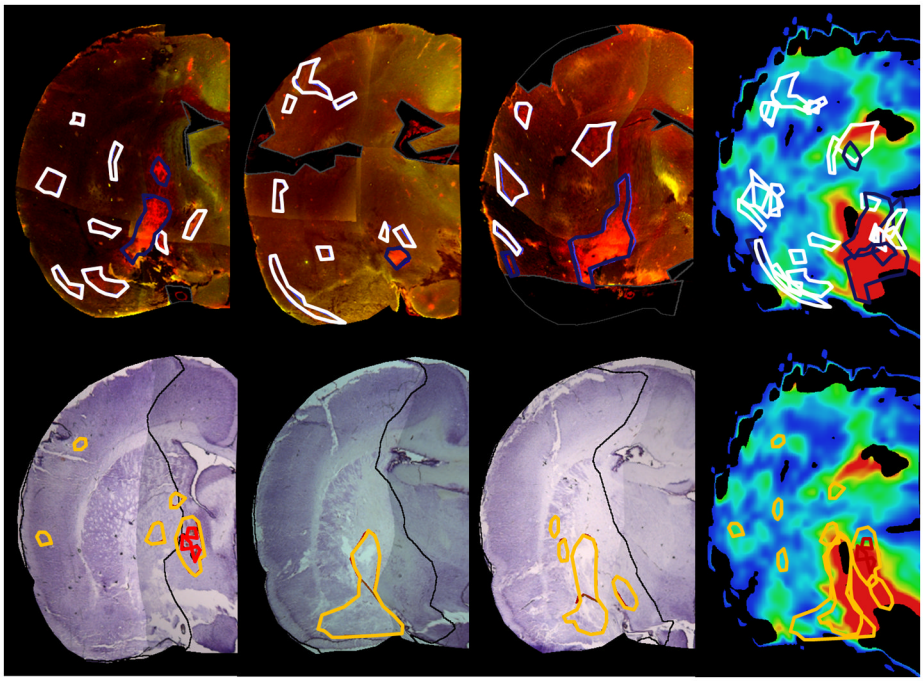

Figure 1. Blood-brain barrier disruption observed by Patlak permeability measurements on a 2mm-thick MR slice in a representative animal and corresponding histological slides

The first row shows three consecutive Evans blue slices, the second row shows three consecutive Cresyl Violet stained sections, which are matched to one MRI slice with permeability measurements. Evans blue and MRI slices as well as Cresyl Violet and MRI slices were individually aligned to the atlas, allowing for the transfer of ROIs identified on histology to the corresponding MRI slice for permeability measurements (strong permeability - blue, weak permeability - white, infarction - black, macroscopic hemorrhage - red, microscopic hemorrhage - yellow). Evans blue extravasation overlap partially with regions of hemorrhagic transformation. Both occurred mainly in the striatal area.

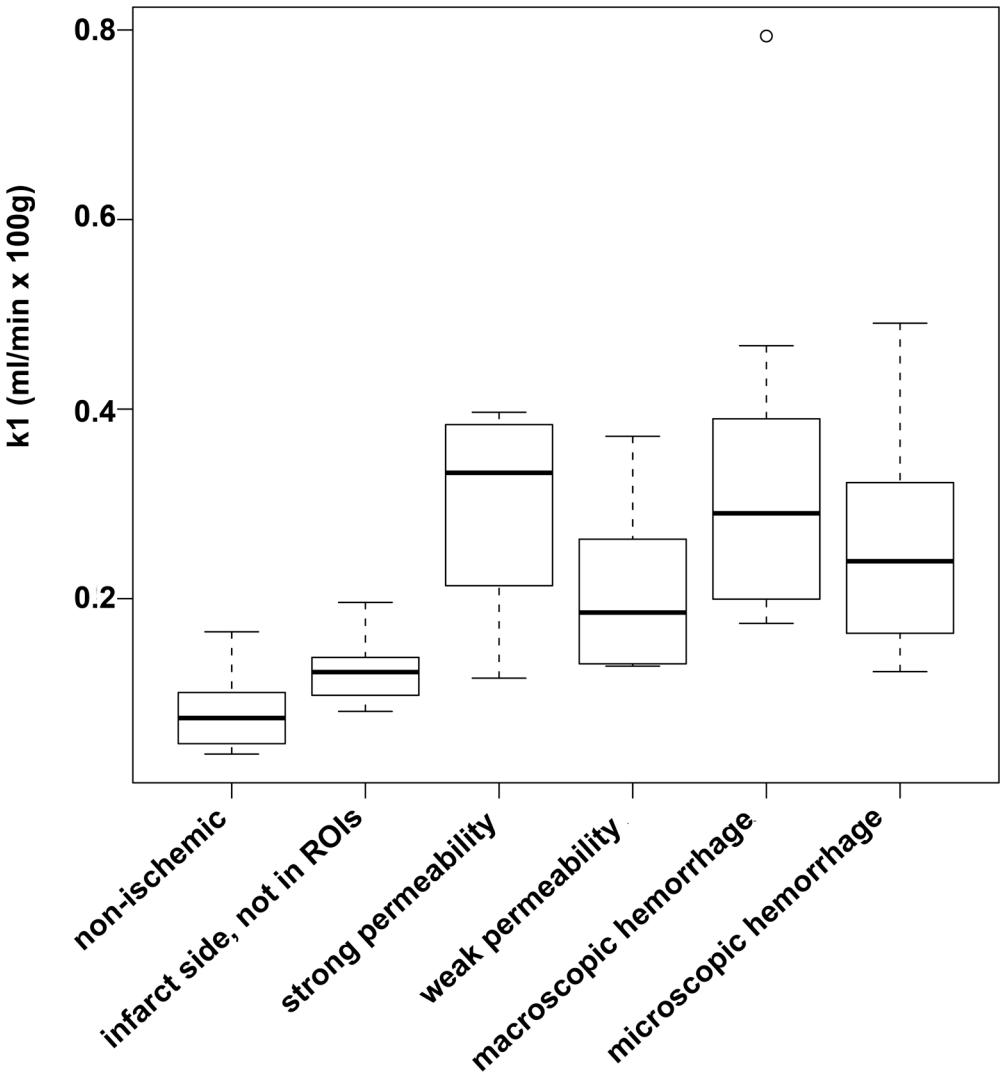

Figure 2.
Box plot of permeability values in the different types of ROIs

Table 1

Volumes of DWI and PWI lesions during occlusion, of infarct and of regions with abnormal permeability at 24h on DWI and at histology, and of macroscopic and microscopic hemorrhage. The Volumes of affected territory are expressed as a fraction of the total volume of the corresponding hemisphere. Comparing SHR rats and Wistar rats revealed no statistically significant differences either in infarct or perfusion lesion sizes. Hemorrhage was more frequent and larger in SHR rats.

Breed	**SHR**				**Wistar rats**				
	Avg	**SD**	**Min**	**Max**	**Avg**	**SD**	**Min**	**Max**	**p-value**
DWI lesion during occlusion	0.73	0.05	0.67	0.77	0.59	0.21	0.32	0.78	>0.99
PWI lesion during occlusion	0.65	0.09	0.77	0.75	0.68	0.05	0.63	0.74	0.79
% of restored normal perfusion after reperfusion compared to PWI lesion during occlusion	0.87	0.10	0.72*	0.99	0.95	0.04	0.91	0.99	0.20
DWI lesion @ 24h	0.79	0.06	0.73	0.92	0.80	0.06	0.71	0.85	0.65
Infarct on Cresyl-violet	0.79	0.03	0.73	0.83	0.82	0.08	0.74	0.93	0.53
Region with abnormal permeability (increased *k*1-values) @ 24h	0.05	0.05	0.00	0.12	0.05	0.08	0.00	0.17	0.70
Strong EB extravasation	0.02	0.02	0.01	0.05	0.05	0.04	0.01	0.11	0.41
Weak EB extravasation	0.03	0.02	0.002	0.05	0.07	0.05	0.01	0.13	0.23
Macroscopic hemorrhage	0.01	0.01	0.001	0.02	0.001	0.001	0.0002	0.0020	**0.02**
Microscopic hemorrhage	0.05	0.04	0.008	0.11	0.02	0.02	0.008	0.04	0.22

*One SHR rat, which did not reperfuse was excluded from the calculation. A reperfusion of 21% occurred in one SHR rat with a major macroscopic bleed: this rat was also excluded from the calculation because it was felt that the large hemorrhage interfered with the calculation of an accurate reperfusion rate. All other SHR rats showed a reperfusion rate of 72% to 99%.

Table 2

Differences in estimated marginal means (± standard error) of permeability values in the different types of ROIs, which were extracted from the mixed linear regression model are shown in the upper right triangular matrix, the corresponding p-values in the lower left triangular matrix.

Differences in estimated marginal means±SE/ p-values	**Non-ischemic**	**Strong Evans blue extravasation**	**Weak Evans blue extravasation**	**Macroscopic hemorrhage**	**Microscopic hemorrhage**
non-ischemic	-	**−0.105±0.025**	**−0.036±0.008**	**−0.160±0.048**	**−0.070±0.020**
strong extravasation	**0.001**	-	**0.069±0.024**	−0.055±0.052	0.035±0.030
weak extravasation	**0.004**	**0.018**	-	−0.124±0.048	−0.034±0.020
macroscopic hemorrhage	**0.013**	0.317	0.038	-	0.090±0.051
microscopic hemorrhage	**0.009**	0.259	0.131	0.115	-